Title

Caveolin1 Is Required for Th1 Cell Infiltration, but Not Tight Junction Remodeling, at the Blood-Brain Barrier in Autoimmune Neuroinflammation

Journal

Cell Reports, 21(8)

ISSN

2639-1856

Authors

Lutz, Sarah E
Smith, Julian R
Kim, Dae Hwan
et al.

Publication Date

2017-11-01

DOI

10.1016/j.celrep.2017.10.094

Peer reviewed

Article

Cell Reports

Caveolin1 Is Required for Th1 Cell Infiltration, but Not Tight Junction Remodeling, at the Blood-Brain Barrier in Autoimmune Neuroinflammation

Graphical Abstract

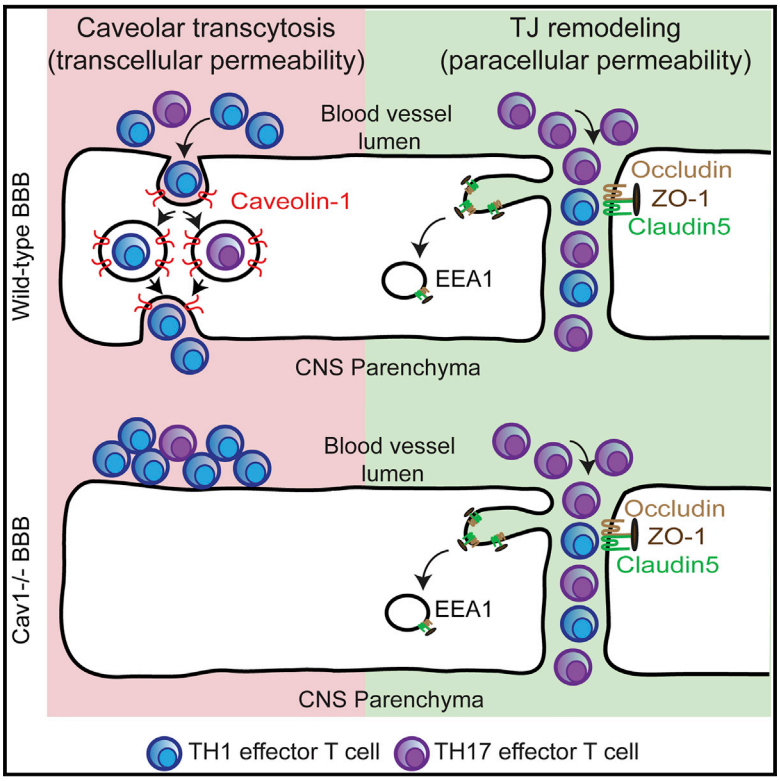

Highlights

- Intravital two-photon microscopy shows that TJ remodeling precedes the onset of EAE
- Caveolar transcytosis is not required for endothelial TJ remodeling *in vivo*
- Effector T cell subsets use distinct mechanisms to cross the inflamed BBB
- Caveolar transcytosis is required for Th1, but not Th17, cell entry into the CNS

Authors

Sarah E. Lutz, Julian R. Smith, Dae Hwan Kim, ..., Jennifer M. Bates, Sunil P. Gandhi, Dritan Agalliu

Correspondence

selutz@uic.edu (S.E.L.), da191@cumc.columbia.edu (D.A.)

In Brief

Autoreactive T cell trafficking into the CNS exacerbates multiple sclerosis; yet how these cells enter the CNS remains unclear. Lutz et al. demonstrate that Caveolin1 exacerbates disease pathogenesis by promoting selective trafficking of Th1 cells across the BBB independently of tight junction remodeling.

Lutz et al., 2017, Cell Reports *21*, 2104–2117
November 21, 2017
https://doi.org/10.1016/j.celrep.2017.10.094

CellPress

OPEN ACCESS
CellPress

Cell Reports
Article

Caveolin1 Is Required for Th1 Cell Infiltration, but Not Tight Junction Remodeling, at the Blood-Brain Barrier in Autoimmune Neuroinflammation

Sarah E. Lutz,[1,7,*] Julian R. Smith,[1] Dae Hwan Kim,[5] Carl V.L. Olson,[5] Kyle Ellefsen,[5] Jennifer M. Bates,[6] Sunil P. Gandhi,[5] and Dritan Agalliu[1,2,3,4,8,*]
[1]Department of Neurology
[2]Department of Pathology & Cell Biology
[3]Department of Pharmacology
[4]Columbia Translational Neuroscience Initiative
Columbia University Medical Center, New York, NY 10032, USA
[5]Department of Neurobiology and Behavior
[6]Institute for Immunology
University of California, Irvine, Irvine, CA 92697, USA
[7]Present address: Department of Anatomy and Cell Biology, University of Illinois at Chicago College of Medicine, Chicago, IL 60612, USA
[8]Lead Contact
*Correspondence: selutz@uic.edu (S.E.L.), da191@cumc.columbia.edu (D.A.)
https://doi.org/10.1016/j.celrep.2017.10.094

SUMMARY

Lymphocytes cross vascular boundaries via either disrupted tight junctions (TJs) or caveolae to induce tissue inflammation. In the CNS, Th17 lymphocytes cross the blood-brain barrier (BBB) before Th1 cells; yet this differential crossing is poorly understood. We have used intravital two-photon imaging of the spinal cord in wild-type and caveolae-deficient mice with fluorescently labeled endothelial tight junctions to determine how tight junction remodeling and caveolae regulate CNS entry of lymphocytes during the experimental autoimmune encephalomyelitis (EAE) model for multiple sclerosis. We find that dynamic tight junction remodeling occurs early in EAE but does not depend upon caveolar transport. Moreover, Th1, but not Th17, lymphocytes are significantly reduced in the inflamed CNS of mice lacking caveolae. Therefore, tight junction remodeling facilitates Th17 migration across the BBB, whereas caveolae promote Th1 entry into the CNS. Moreover, therapies that target both tight junction degradation and caveolar transcytosis may limit lymphocyte infiltration during inflammation.

INTRODUCTION

During inflammation, immune cells cross blood vessels of multiple organs to mount an appropriate immune response. Immune cell trafficking across blood vessels is controlled by both cell junctions and vesicles that regulate transport between or within endothelial cells (Komarova et al., 2017). During CNS autoimmune diseases, leukocytes migrate across several pathways to reach the CNS parenchyma. These include a vascular route through the blood-brain barrier (BBB) or blood-spinal cord barrier (BSCB), the blood-cerebrospinal fluid route through an epithelial barrier present in the choroid plexus, and the meningeal lymphatic route on the surface of the brain (Daneman and Engelhardt, 2017; Louveau et al., 2017; Platt et al., 2017). The BBB is characterized by impermeable tight junctions (TJs) and reduced transcellular transcytosis (Lampugnani et al., 2015; Reese and Karnovsky, 1967). Immune cells can extravasate through either tight junctions (paracellular migration) or endothelial vesicles (transcellular migration) (Engelhardt and Wolburg, 2004; Martinelli et al., 2014). Among the various immune cell subtypes, T helper 1 (Th1) and T helper 17 (Th17) lymphocytes are distinguished by unique effector cytokines that damage axons, oligodendrocytes, and the neurovasculature (Rostami and Ciric, 2013; Simmons et al., 2014; Stromnes et al., 2008). Moreover, Th17 cells enter the CNS before Th1 cells in experimental autoimmune encephalomyelitis (EAE) (Murphy et al., 2010; Rothhammer et al., 2011). However, it is unknown whether they employ similar or distinct mechanisms to cross endothelial barriers.

Claudin3, Claudin5, Claudin12, and Occludin are critical junctional proteins that normally restrict paracellular movement of small molecules across endothelial cell barriers (Nag, 2003; Nitta et al., 2003). These proteins are disrupted in inflammatory diseases, including multiple sclerosis and its animal model EAE (Bennett et al., 2010; Kirk et al., 2003). Tight junction disruption precedes overt lesion formation and correlates with clinical severity of EAE (Alvarez et al., 2015; Fabis et al., 2008). Moreover, endothelial tight junction degradation promotes paracellular leukocyte migration (Reijerkerk et al., 2008; Winger et al., 2014), whereas overexpression of Claudin1 is protective for EAE (Pfeiffer et al., 2011). Endothelial tight junctions also prevent serum proteins such as fibrinogen from crossing the BBB, thereby conferring disease protection (Ryu et al., 2015). Tight junctions are highly dynamic *in vivo* in both the cerebral cortex and the intestinal epithelia, and their turnover is increased during inflammation (Knowland et al., 2014; Marchiando et al., 2010).

Although barrier disruption promotes neuroinflammation by enabling inflammatory proteins and leukocytes to access the CNS, how dynamic remodeling of tight junctions correlates with disease pathogenesis and its importance for immune cell trafficking remain unclear.

A second mechanism controlling BBB permeability is endocytic and transcytotic transport. In the CNS endothelium, most endocytic vesicles are non-clathrin-coated caveolae containing Caveolin1 (Cav1) (Kovtun et al., 2015; Nag, 2003). Both the expression of Caveolin1 (Shin et al., 2005; Wu et al., 2016) and the density of endocytotic vesicles in CNS endothelium increase during acute multiple sclerosis and EAE (Brown, 1978; Claudio and Brosnan, 1992). Endothelial caveolae may provide a migratory route for myelin-specific T cells into the CNS (Raine et al., 1990) because of clustering of adhesion molecules (Carman and Martinelli, 2015; Millán et al., 2006). Caveolar activity also enhances leukocyte migration across the meninges (Santizo et al., 2002). Caveolae regulate cytokine-induced tight junction turnover in epithelial and endothelial cells (Marchiando et al., 2010; Stamatovic et al., 2009; Sun et al., 2009). However, how caveolae regulate Th17 versus Th1 cell trafficking and tight junction remodeling at the BBB during EAE is poorly understood.

Here we examine how BBB components are disrupted *in vivo* during EAE and which routes are used by distinct effector T cell subtypes to enter the CNS. We use intravital two-photon microscopy in transgenic (*Tg*) *eGFP-Claudin5*$^{+/-}$ mice (Knowland et al., 2014) to visualize dynamic changes in tight junctions at the BSCB during EAE. We find that tight junction remodeling precedes the onset of disease and barrier permeability. Moreover, mice that lack caveolae have reduced EAE clinical severity and a selective decrease in BSCB permeability to Th1 cells yet display no changes in dynamic tight junction remodeling. These findings suggest that during neuroinflammation, caveolae-independent tight junction remodeling facilitates Th17 lymphocyte transmigration across the BBB, whereas caveolae regulate the entry of Th1 lymphocytes into the CNS.

RESULTS

Live Imaging of Tight Junction Structural Changes in Healthy Spinal Cord Vessels

To document real-time changes in tight junction structure in the spinal cord microvasculature during EAE, we used intravital two-photon microscopy in transgenic *eGFP-Claudin5*$^{+/-}$ transgenic mice that express a fusion of EGFP to Claudin5 in endothelial cells (Knowland et al., 2014). We performed dorsal laminectomy at lumbar level 1 (L1) to expose the spinal cord and time-lapse imaging of endothelial tight junctions over 45-min intervals (n = 6–7 mice/group) (Figures 1A and 1B). We focused on post-capillary venules because leukocyte transmigration occurs primarily in such vessels during EAE and is associated with loss of Claudin5 (Paul et al., 2013). In healthy mice, EGFP-positive tight junctions are mostly linear (Figures 1E and 1F). In the dorsal white matter, 25% of tight junctions in healthy blood vessels show protrusions (bulbous extensions of 1–5 μm extending from the major tight junction segment axis); however, only 5% of protrusions rapidly remodel (appear or disappear during imaging) (Figures 1C, 1E, 1F, 1M, and 1N; Movie S1). Moreover, healthy tight junctions exhibit few gaps (1.8%) (Figures 1D–1F and 1O) or tortuous, irregular non-linearity (4.6%) (Figures 1C and 1P), which is reminiscent of junctions in cells lacking ZO-1 and ZO-3 proteins (Umeda et al., 2006). Thus, only a small fraction (5%) of endothelial tight junction segments undergo dynamic remodeling in the healthy spinal cord.

Dynamic Remodeling of Tight Junctions Precedes Disease Onset and Barrier Permeability during EAE

We next asked how tight junction remodeling correlates with BBB permeability during EAE. We induced active EAE with myelin oligodendrocyte glycoprotein peptide 35–55 ($MOG_{35–55}$) (Lutz et al., 2012) in Tg *eGFP-Claudin5*$^{+/-}$ mice and assessed tight junction structure by two-photon microscopy at three stages of disease: (1) before clinical signs (EAE score 0, 6–7 days post-immunization [dpi]), (2) in mice with tail paralysis (EAE score 1, 10 days post-immunization), and (3) in mice with hindlimb weakness or paralysis (EAE score 2–3, 13–15 days post-immunization). All animals with EAE have significantly more protrusions than healthy controls (i.e., ~70% in all stages of EAE versus ~25% in controls; $p < 0.001$, one-way ANOVA with Tukey's multiple comparison) (Figures 1G–1M). Approximately 40% of tight junction protrusions in post-capillary venules during EAE undergo rapid remodeling (Figures 1G–1N; Movie S2). Similarly, tight junction segments with gaps and tortuous segments are predominant at EAE score 1 (55.8% and 56.2%, respectively) and EAE score 2 (56.5% and 64.6%, respectively), but these defects are absent in mice before onset of clinical signs (EAE score 0, 14.5% and 14.3%, respectively) (Figures 1G–1L, 1O, and 1P) (data not shown). Therefore, tight junction dynamic remodeling precedes gap formation. Internalized tight junction protrusions localize *in vivo* with the early endosome marker EEA-1, but not clathrin (Figure S1). Similar to healthy mice, complete Freund's adjuvant (CFA) and pertussis toxin-treated control mice, which do not develop disease, exhibit only static protrusions (50%), not dynamic protrusions (7.7%), in tight junction segments, with few gaps (3.7%) or irregular segments (10%); these frequencies are similar to those in healthy mice (Figures 1M–1P). Thus, tight junction dynamic remodeling and instability are features of active EAE.

Caveolin1 Is Not Required for Tight Junction Structural Changes in EAE Spinal Cord Vessels

Tight junction stability may be regulated by caveolae, a class of membrane invaginations that require Caveolin1 (Cheng and Nichols, 2016). Caveolae regulate endocytosis of tight junction proteins and barrier permeability in brain endothelial cells *in vitro* (Song et al., 2007; Stamatovic et al., 2009); however, it is unknown whether caveolae perform similar functions at the BBB *in vivo*. To address this, we immunized *Cav1*$^{-/-}$ mice (Razani et al., 2001) with $MOG_{35–55}$ and assessed disease and tight junction remodeling. EAE-induced *Cav1*$^{-/-}$ mice showed reduced disease severity compared to wild-type (WT) littermates (n = 34, wild-type; n = 32, *Cav1*$^{-/-}$; $p < 0.01$, two-way repeated-measure ANOVA with Sidak's multiple comparison test) (Figure 2A). The maximum score attained by *Cav1*$^{-/-}$ mice was lower than that attained by wild-type mice ($p < 0.001$, Mann-Whitney comparison of medians) despite similar disease

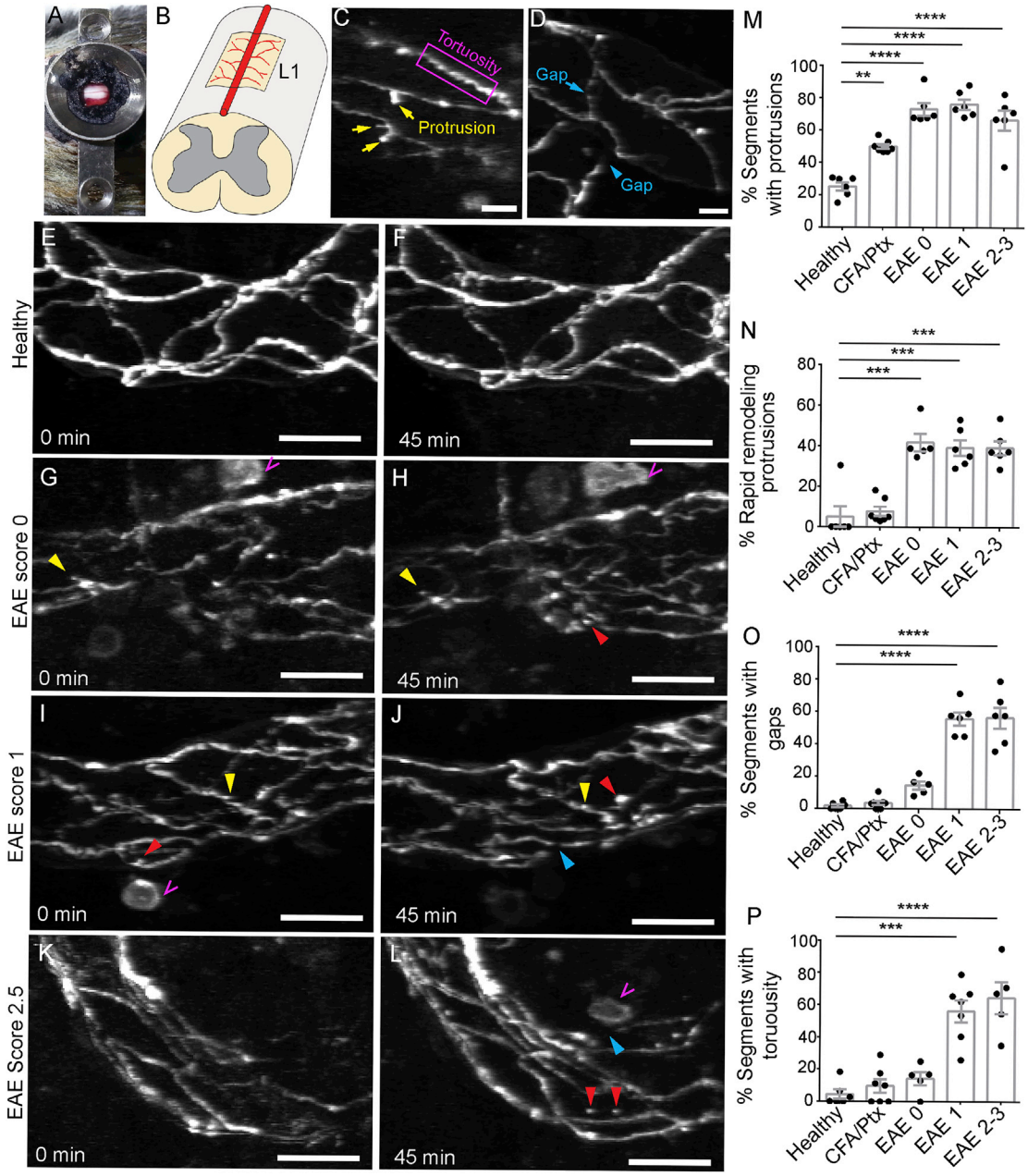

Figure 1. Dynamic Tight Junction Changes in Spinal Cord Blood Vessels during EAE Revealed by Intravital Two-Photon Microscopy of Transgenic *eGFP-Claudin5*$^{+/-}$ Mice

(A and B) Dorsal laminectomy (A) and diagram of the imaging window (B) in the dorsal white matter of lumbar level 1 (L1) spinal cord in mice.

(C and D) Examples of EGFP-positive tight junction (TJ) protrusions (C), tortuosity (C), and gaps (D).

(E–L) Maximum intensity projections of two sequential time-lapse images of spinal cord venules in healthy (E and F, n = 6), preclinical (G and H, n = 5, EAE score 0), mild EAE (I and J, n = 6, score 1), and severe EAE (K and L, n = 6, score 2–3) transgenic *eGFP-Claudin5*$^{+/-}$ mice at 0- and ~45-min intervals. The 0 min timepoints are shown in (E), (G), (I), and (K); 45 min timepoints are shown in (F), (H), (J), and (L). Yellow arrows show static tight junction protrusions, red arrows point to dynamic tight junction protrusions that appear or disappear during the imaging period, blue arrows show tight junction gaps, and magenta open arrows point to myeloid or lymphoid cells.

(M–P) Bar graphs show percentages of tight junction segments with protrusions (M), dynamic protrusions (N), gaps (O), and tortuosity (P). Each dot represents the mean of multiple fields from a single mouse.

Bar graphs show mean ± SEM, *p < 0.05, **p < 0.01, ***p < 0.001, one-way ANOVA. Scale bars, 20 μm (C and E–L) and 10 μm (D). See also Figure S1.

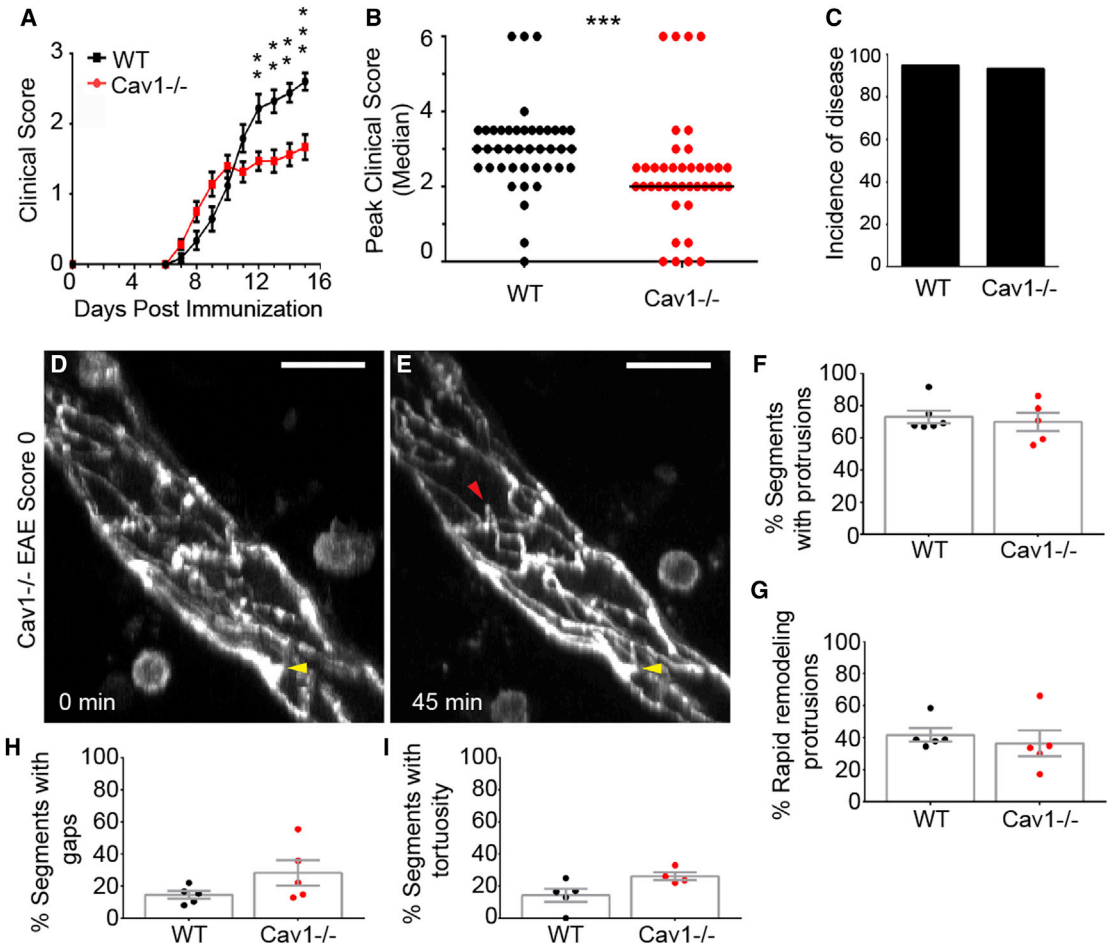

Figure 2. Caveolin1-Deficient Mice Display Attenuated EAE but No Changes in Tight Junction Remodeling

(A) Clinical EAE scores in wild-type (n = 34) and *Cav1*$^{-/-}$ (n = 32) littermate mice. *Cav1*$^{-/-}$ mice have less severe clinical scores at the indicated times (12–15 days post-immunization; **p < 0.01, ***p < 0.001, two-way repeated-measure ANOVA). The graph excludes mice that died during the experiment (n = 0, wild-type; n = 2, *Cav1*$^{-/-}$).

(B) Scatterplot of maximum clinical scores attained by each mouse. *Cav1*$^{-/-}$ mice had less severe scores (p < 0.001, Mann-Whitney comparison of medians).

(C) Bar graph of disease incidence.

(D and E) Maximum intensity projections of time-lapse imaging recordings at 0 min (D) and 45 min (E) for spinal cord venules in transgenic *eGFP-Claudin5*$^{+/-}$, *Cav1*$^{-/-}$ mice at EAE score 0 (n = 5–6). Yellow arrows show static protrusions, and red arrows point to dynamic protrusions that appear or disappear during the imaging period. Scale bars, 20 μm.

(F–I) Bar graphs show percentages of tight junction segments with protrusions (F), dynamic protrusions (G), gaps (H), and tortuosity (I) between Tg *eGFP-Claudin5*$^{+/-}$ and Tg *eGFP-Claudin5*$^{+/-}$, *Cav1*$^{-/-}$ mice. No differences were found for tight junction structural features between the two genotypes.

See also Figure S2.

incidence (Figures 2B and 2C). The peripheral immune response to MOG was unchanged in *Cav1*$^{-/-}$ mice compared to wild-type mice (Figures S2A–S2K), consistent with a recent report (Wu et al., 2016). In a subset of animals examined up to 25 days post-immunization, the clinical trend remained the same (n = 5 per group; p < 0.001) (Figure S2L). *Cav1*$^{-/-}$ mice with EAE had slightly better myelin preservation in the thoracic spinal cord than did wild-type mice with EAE (Figures S2M–S2O). However, there was no difference in oligodendrocyte apoptosis (Figures S2P–S2R), suggesting that caveolae do not influence oligodendrocyte death.

Caveolae Are Not Required *In Vivo* during EAE for Tight Junction Dynamic Remodeling and Permeability to Small Molecules

We used intravital two-photon microscopy to compare tight junction dynamic remodeling *in vivo* between transgenic *eGFP-Claudin5*$^{+/-}$ *Cav1*$^{-/-}$ and *eGFP-Claudin5*$^{+/-}$ mice at an early stage of EAE (score 0, 7 days post-immunization), when we first observe tight junction dynamic remodeling (Figures 1G, 1H, and 1M–1P). Transgenic *eGFP-Claudin5*$^{+/-}$ *Cav1*$^{-/-}$ and *eGFP-Claudin5*$^{+/-}$ mice had similar frequencies of static and dynamic protrusions, gaps, or tortuosities (Figures 2D–2I). To correlate

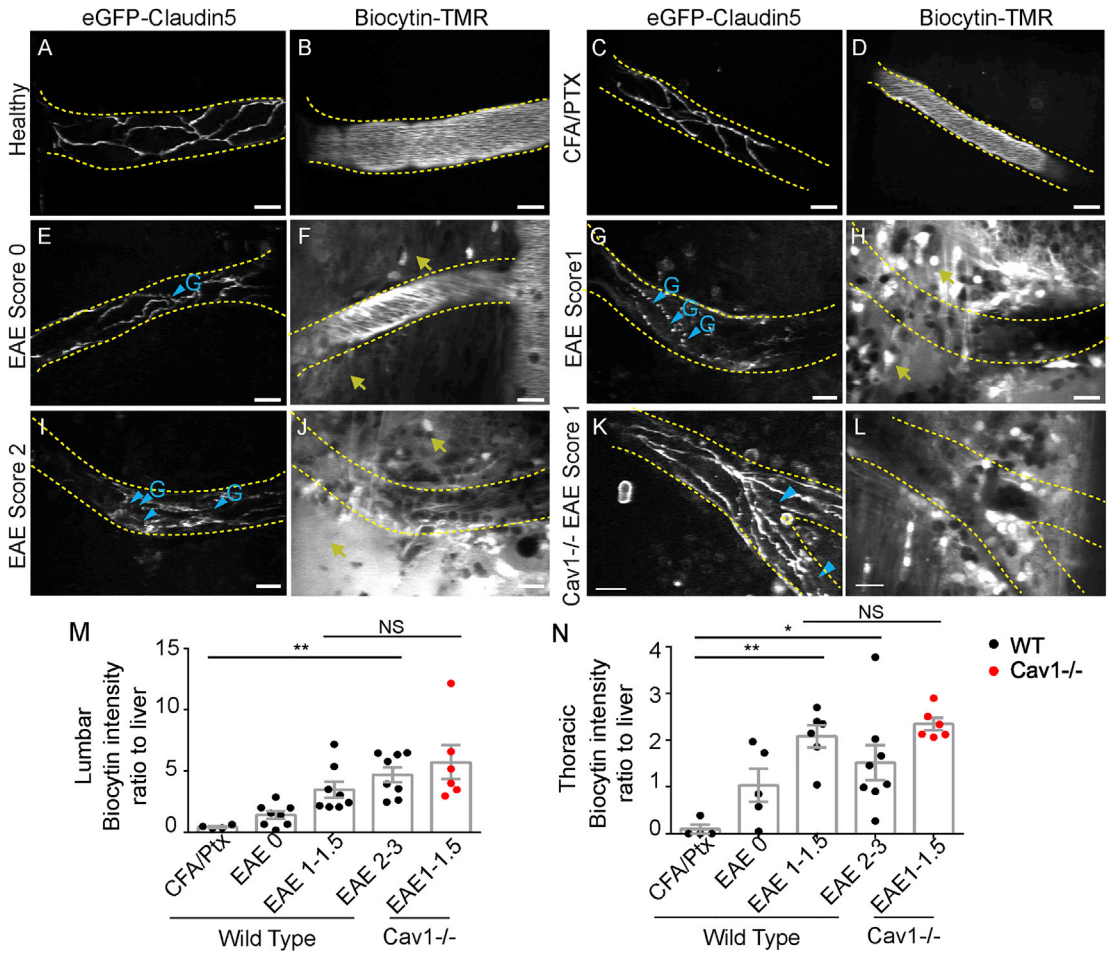

Figure 3. Paracellular BBB Leakage in Spinal Cord Blood Vessels

Biocytin-TMR was intravenously injected into transgenic *eGFP-Claudin5*$^{+/-}$ and *eGFP-Claudin5*$^{+/-}$, *Cav1*$^{-/-}$ mice before *in vivo* imaging with two-photon microscopy.

(A–D) Healthy and CFA and pertussis toxin control transgenic *eGFP-Claudin5*$^{+/-}$ mice had continuous tight junction segments (A and C), and biocytin-TMR was confined within the lumen of spinal cord blood vessels (B and D).

(E and F) Transgenic *eGFP-Claudin5*$^{+/-}$ mice with EAE score 0 had some tight junction gaps (E, blue arrowheads) and minimal biocytin-TMR leakage outside of blood vessels (F, yellow arrows).

(G–J) Transgenic *eGFP-Claudin5*$^{+/-}$ mice with EAE score 1 (G and H) and EAE score 2 (I and J) had multiple tight junction gaps (G and I, blue arrowheads) and extensive extravascular biocytin-TMR in the spinal cord (H and J, yellow arrows).

(K and L) Transgenic *eGFP-Claudin5*$^{+/-}$, *Cav-1*$^{-/-}$ mice with EAE score 1 had multiple tight junction gaps (blue arrowheads, K) and extravascular biocytin-TMR (L).

(M and N) Graphs of biocytin-TMR fluorescence intensity in the lumbar (M) and thoracic (N) spinal cord normalized to fluorescence intensity in the liver *ex vivo* (n = 4, CFA and pertussis toxin control; n = 7, EAE score 0; n = 6, EAE score 1; n = 8, EAE score 2–3).

Scale bars, 20 μm. See also Figure S3.

tight junction structural changes with loss of BSCB function *in vivo*, we injected transgenic *eGFP-Claudin5*$^{+/-}$ EAE, *eGFP-Claudin5*$^{+/-}$ *Cav1*$^{-/-}$ EAE, CFA and pertussis toxin controls, and healthy *eGFP-Claudin*$^{5+/-}$ mice intravenously with 5-(and-6-)tetramethylrhodamine biocytin (biocytin-TMR, 869 Da), which crosses the BBB when tight junctions are disrupted (Dileepan et al., 2016; Knowland et al., 2014; Lengfeld et al., 2017). We visualized biocytin-TMR in the spinal cord by two-photon microscopy and then normalized it *ex vivo* to liver accumulation from the same animal (Figure 3). The tracer is retained within blood vessels in healthy and CFA-treated mice (Figures 3A–3D, 3M, and 3N). Leakage from vessels is mild at EAE score 0 (Figures 3E, 3F, 3M, and 3N) and pronounced in symptomatic mice, particularly at sites of tight junction gaps (EAE score 1–3) (Figures 3G–3J, 3M, and 3N). However, there is no difference in biocytin leakage across the BSCB between transgenic *eGFP-Claudin5*$^{+/-}$ *Cav1*$^{-/-}$ and *eGFP-Claudin5*$^{+/-}$ mice (Figures 3K–3N).

We also measured parenchymal deposition of the serum protein fibrinogen (approximately 340 kDa) by immunofluorescence.

Fibrin accumulation was minimal in CFA and *pertussis* toxin (Ptx) controls and EAE score 0–1 mice (Figures S3A–S3I, S3P, and S3Q). Mice with clinical EAE scores > 2 had significantly elevated fibrinogen at thoracic and lumbar levels of the spinal cord (Figures S3J–S3L, S3P, and S3Q), with regions of leukocyte infiltration displaying greatest leakage (Figures S3I, S3L, and S3O). Transgenic *eGFP-Claudin5*$^{+/-}$ *Cav1*$^{-/-}$ EAE mice and *eGFP-Claudin5*$^{+/-}$ EAE mice have similar levels of fibrinogen leakage (Figures S3M–S3Q), consistent with tracer leakage across the BSCB. Thus, the presence of tight junction gaps correlates closely with paracellular BSCB permeability in both transgenic *eGFP-Claudin5*$^{+/-}$ EAE mice and *eGFP-Claudin5*$^{+/-}$ *Cav1*$^{-/-}$ EAE mice.

We next measured leakage of albumin-Alexa Fluor 594, a 66 kDa protein that can undergo caveolar transcytosis (Tiruppathi et al., 1997), during active $MOG_{35–55}$ EAE in wild-type and *Cav1*$^{-/-}$ mice. We used confocal microscopy to assess endothelial- and parenchymal-associated albumin (Knowland et al., 2014; Lengfeld et al., 2017). Healthy and CFA and *pertussis* toxin control mice exhibit minimal albumin-Alexa Fluor 594 uptake into both lumbar and thoracic spinal cords (Figures 4A–4D, 4M, and 4N; Figures S4A and S4B), consistent with previous studies (Al-Izki et al., 2012; Tonra et al., 2001). Both endothelial- and parenchyma-associated albumin are significantly increased at EAE score 2–3.5 (Figures 4G, 4H, 4M, and 4N). Albumin transport across the endothelium depends on caveolar transcytosis in some peripheral tissues and during ischemic stroke in the brain (Knowland et al., 2014; Razani et al., 2001). As expected, the absence of Cav1 prevents albumin leakage in spinal cords of healthy mutant mice (Figures 4I, 4J, 4M, and 4N; Figures S4A and S4B). However, *Cav1*$^{-/-}$ mice with EAE have levels of endothelium- or parenchymal-associated albumin similar to those of their wild-type littermates using score-matched EAE mice (Figures 3K–3N). Thus, BSCB permeability to larger molecules such as albumin increases at severe EAE through caveolae-independent routes.

Loss of Caveolin1 Selectively Reduces Th1 Cell Infiltration into the CNS

We tested the role of caveolar transcytosis in T cell diapedesis. In contrast with a recent study (Wu et al., 2016), we found that *Cav1*$^{-/-}$ mice with EAE have similar $CD4^+$ T cell numbers in both meningeal and parenchymal compartments 15 days post-immunization compared to wild-type mice with EAE by immunostaining (two-way Student's t test) (Figures 5A–5G). To understand how loss of Cav1 reduces the severity of EAE, we examined lymphocyte subtypes in the spinal cord using flow cytometry. We found that although the total number of infiltrating T and B cells were similar between wild-type and *Cav1*$^{-/-}$ mice with active EAE, the ratio of Th1 to Th17 subtypes was significantly altered (Figures 5H–5Q). Spinal cords of *Cav1*$^{-/-}$ mice had a selective decrease in interferon γ (IFN-γ)-producing Th1 cells and increased interleukin (IL)-17A-producing Th17 cells (Figures 5I, 5J, 5N, and 5O). No differences were found for IL-$17a^+$ IFN-γ^+ double-positive cells (Figure 5P) or $CD19^+$ B cells (Figures 5K and 5Q). To confirm these findings, we assessed transmigration of Th1- or Th17-enriched populations of T cells (Figures S5A–S5C) across cultured primary brain endothelial cell (BEC) monolayers isolated from either wild-type or *Cav1*$^{-/-}$ mice (Figure 6). We found that the *Cav1*$^{-/-}$ endothelium showed a 93.5% reduction in transcellular transmigration and 49% reduction in paracellular transmigration of Th1 lymphocytes (*$p < 0.05$) (Figures 6A–6E and 6J). The caveolae inhibitor methyl-β-cyclodextrin (MβCD) also suppressed Th1 transcellular transmigration across wild-type brain endothelial cells (Figures S5D–S5G). Consistent with our findings *in vivo*, there was no impairment in Th17 lymphocyte migration across *Cav1*$^{-/-}$ endothelium (Figures 6F–6J). Thus, caveolae play an important role in allowing Th1 cell entry into the CNS during neuroinflammation, whereas Th17 cells primarily enter the CNS via disrupted tight junctions. Furthermore, caveolae are not required for dynamic remodeling of tight junctions or increased vascular permeability in EAE.

DISCUSSION

In this study, we have examined *in vivo* dynamic remodeling of tight junctions at the BSCB in healthy living mice and during the EAE model of multiple sclerosis. We find that tight junctions in post-capillary venules of the spinal cord are mostly stable in healthy mice (Figures 1M–1P); however, dynamic remodeling of tight junctions and paracellular BSCB leakage increase before onset of EAE and remain high throughout disease. Moreover, endothelial tight junctions rapidly remodel independent of caveolae in neuroinflammation, because tight junctions exhibit similarly dynamic behavior in both wild-type and *Cav1*$^{-/-}$ EAE mice. Finally, we demonstrate that caveolae are essential for transmigration of IFN-γ-producing Th1 cells into the spinal cord during EAE. We discuss the cell biological mechanisms underlying BBB dysfunction in neurological diseases, mechanisms of immune cell infiltration into the CNS through paracellular and transcellular pathways, and relevance for EAE progression.

Multiple studies have suggested that endothelial barriers of the brain, spinal cord, meninges, and choroid plexus are functionally distinct from one another and from those of the peripheral vasculature. The BBB and BSCB differ in both expression of barrier-specific proteins and their functional permeability. Compared to brain, endothelial cells in the spinal cord have decreased adherens junction (AJ) proteins (e.g., Cadherin-5 and α-, β-, and γ-catenin) and tight junction proteins (e.g., Occludin and ZO-1) and a corresponding increase in permeability to low-molecular-weight tracers (Bartanusz et al., 2011). Our intravital imaging studies reveal that tight junctions in white matter spinal cord are ~4-fold more dynamic (Figure 1) than those in the cortex (Knowland et al., 2014). Thus, our findings extend previous observations that endothelial barriers differ in distinct CNS regions. A higher rate of tight junction remodeling in the spinal cord vasculature may contribute to its increased vulnerability to EAE (Cruz-Orengo et al., 2014).

What regulates tight junction remodeling during inflammation? Caveolae have been proposed to promote tight junction endocytosis *in vitro* in CNS and non-CNS endothelial cells, as well as *in vivo* in non-CNS endothelial cells (Chang et al., 2009; Miyawaki-Shimizu et al., 2006; Rosengren et al., 2006; Schubert et al., 2002; Song et al., 2007). However, we find that *Cav1*$^{-/-}$ and wild-type mice exhibit similar kinetics of tight junction remodeling and BSCB vascular leakage to small-molecular-weight

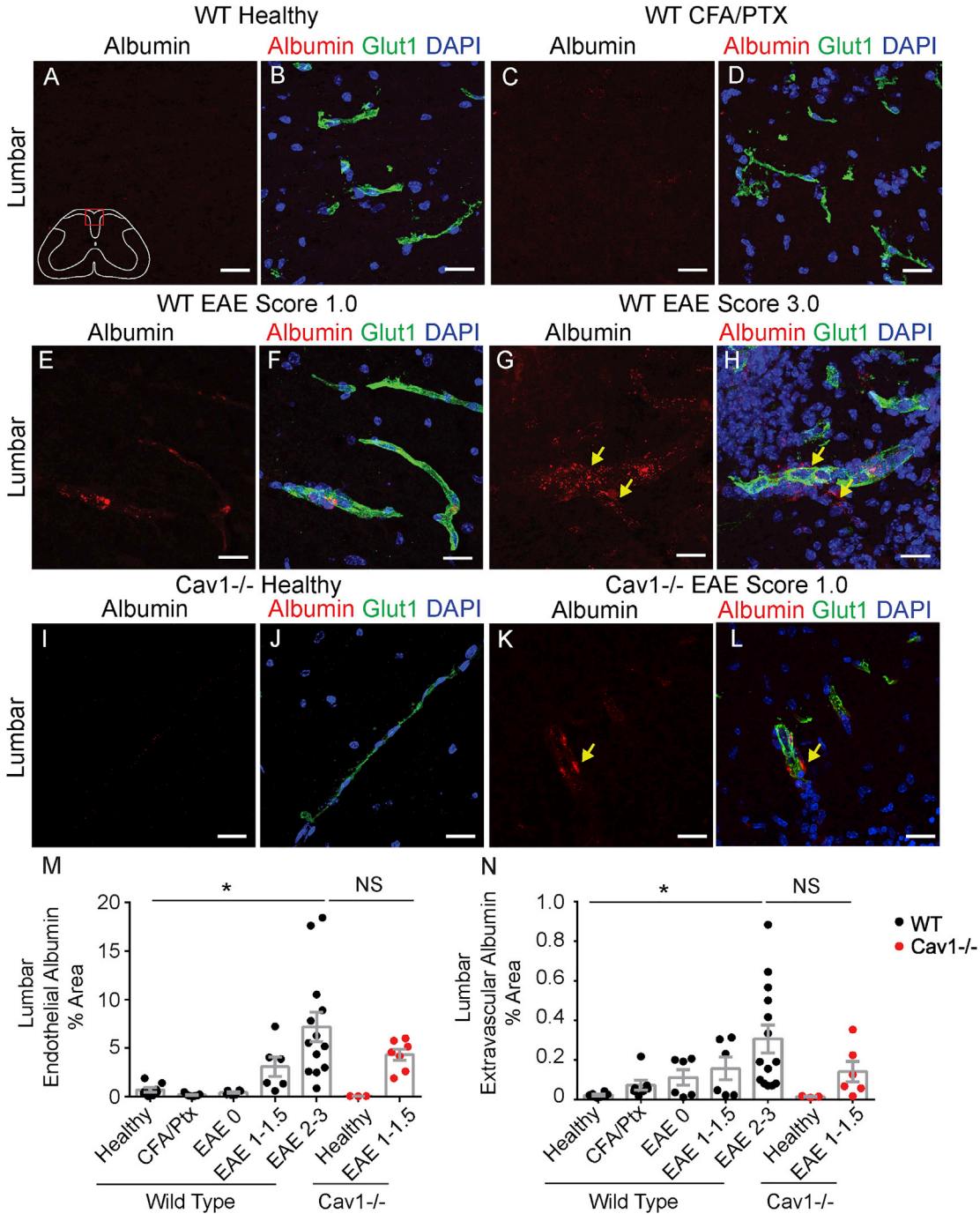

Figure 4. BBB Permeability to Albumin Is Increased at Peak EAE

(A–L) BBB leakage of intravenously injected albumin-Alexa Fluor 594 (red) in lumbar spinal cord sections from healthy (A and B), CFA and pertussis toxin control (C and D), EAE score 1 (E and F) and EAE score 3 (G and H) wild-type mice, and healthy (I and J) and EAE score 1 (K and L) *Cav1*$^{-/-}$ mice. Single channel images for albumin are shown in (A), (C), (E), (G), (I), and (K).The vascular marker Glut1 (green) labels endothelial cells, and DAPI (blue) shows nuclei. Merged psuedocolored images are shown in (B), (D), (F), (H), (J), and (L). Yellow arrows indicate perivascular albumin.

(M and N) Bar graphs of the fraction of endothelium-associated (M) or parenchyma-associated (N) albumin that traversed the BSCB. Each dot represents the mean of multiple fields from a single animal (n = 5–6, healthy; n = 7, CFA and pertussis toxin control; n = 6, EAE score 0; n = 6, EAE score 1–1.5; n = 13–16, EAE score 2–3; n = 3, healthy *Cav1*$^{-/-}$; n = 7, EAE score 1–1.5 *Cav1*$^{-/-}$).

Bar graphs show mean ± SEM, *p < 0.05, one-way ANOVA. Scale bars, 20 μm. See also Figure S4.

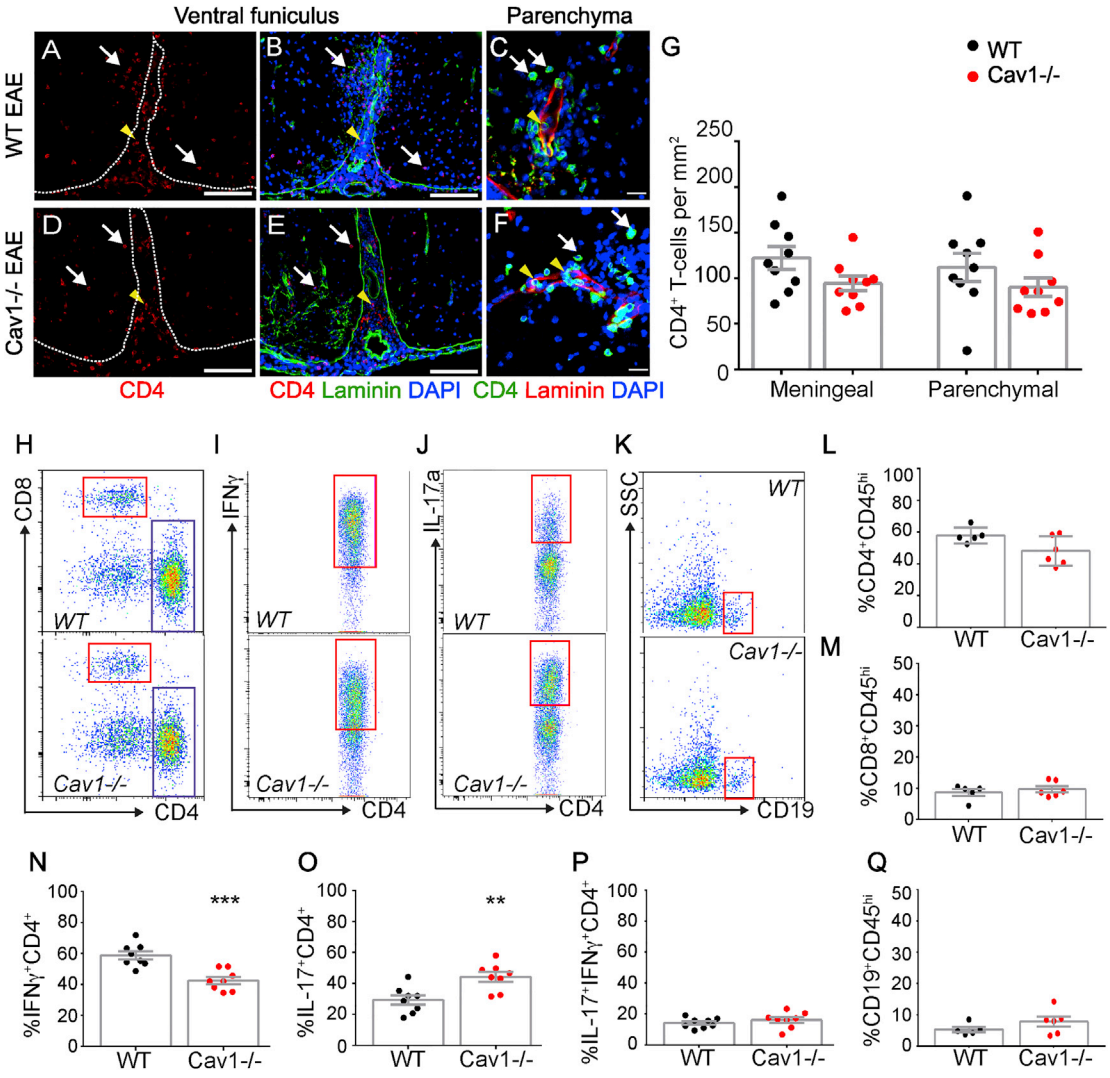

Figure 5. *Cav1*-Deficient Mice Have Reduced IFN-γ-Producing CD4⁺ T Cells in the CNS

(A–F) Immunofluorescence for CD4, laminin, and DAPI in the ventral funiculus (A, B, D, and E) and lateral funiculus (C and F) of wild-type (A, CD4 [red]; B, CD4 [red], laminin [green], DAPI [blue] merged pseudocolored image) and *Cav1*$^{-/-}$ (D, CD4 [red]; E, Cd4 [red], laminin [green], DAPI [blue] merged pseudocolored image) EAE thoracic spinal cords 15 days post-immunization. White arrows point to T cells that have crossed the basal lamina (white dotted line in A and D), whereas yellow arrowheads point to T cells that are located in meningeal or vascular spaces. Scale bars, 200 μm (A, B, D, and E) and 10 μm (C and F).

(G) Bar graphs of CD4⁺ T cell numbers in parenchymal or meningeal compartments of thoracic spinal cords in wild-type and *Cav1*$^{-/-}$ EAE mice 15 days post-immunization. There is no significant difference between genotypes (n = 9, wild-type; n = 9, *Cav1*$^{-/-}$; unpaired two-way Student's t test).

(H–K) Fluorescence-activated cell sorting (FACS) plots for CD8⁺ and CD4⁺ T cells (H), IFN-γ⁺ CD4⁺ T cells (I), IL-17a⁺ CD4⁺ T cells (J), and CD19⁺ B cells (K) isolated from spinal cords of wild-type (n = 8) or *Cav1*$^{-/-}$ (n = 8) mice 15 days post-immunization.

(L and M) Scatterplots of leukocytes gated on viable dye exclusion and high CD45 expression. There were no differences in percentages of infiltrating CD4⁺ CD45^{hi} (L) or CD8⁺ CD45^{hi} (M) between the two genotypes.

(N and O) Scatterplots of the fraction of IFN-γ-producing CD4⁺ Th1 cells (N) and IL-17-producing CD4⁺ Th17 cells (O) in wild-type and *Cav1*$^{-/-}$ EAE mice. Significantly fewer IFN-γ-producing CD4⁺ Th1 cells (N) and significantly more IL-17-producing CD4⁺ Th17 cells (O) were observed in spinal cords of *Cav1*$^{-/-}$ compared to wild-type mice (n = 8, wild-type; n = 8, *Cav1*$^{-/-}$; *$p < 0.05$, **$p < 0.01$, Student's t test).

(P) Scatterplot of the fraction of IL-17⁺ IFN-γ⁺ CD4⁺ T cells in both genotypes. There was no significant difference in the proportion of IL-17⁺ IFN-γ⁺ CD4⁺ T cells.

(Q) Scatterplot of the fraction of CD19⁺ B cells in both genotypes. There was no difference in the fraction of infiltrating CD19⁺ B cells.

tracers (e.g., biocytin-TMR) during EAE. These results extend our prior study that tight junction remodeling is independent of caveolae during barrier breakdown following transient middle cerebral artery occlusion (t-MCAO), a mouse model for ischemic stroke (Knowland et al., 2014). Our data are consistent with caveolae- and clathrin-independent tight junction remodeling or degradation in the CNS endothelium during EAE. A potential mechanism for tight junction degradation could be enhanced endocytotic or macropinocytic remodeling or degradation in response to inflammatory cytokines such as IFN-γ (Bruewer

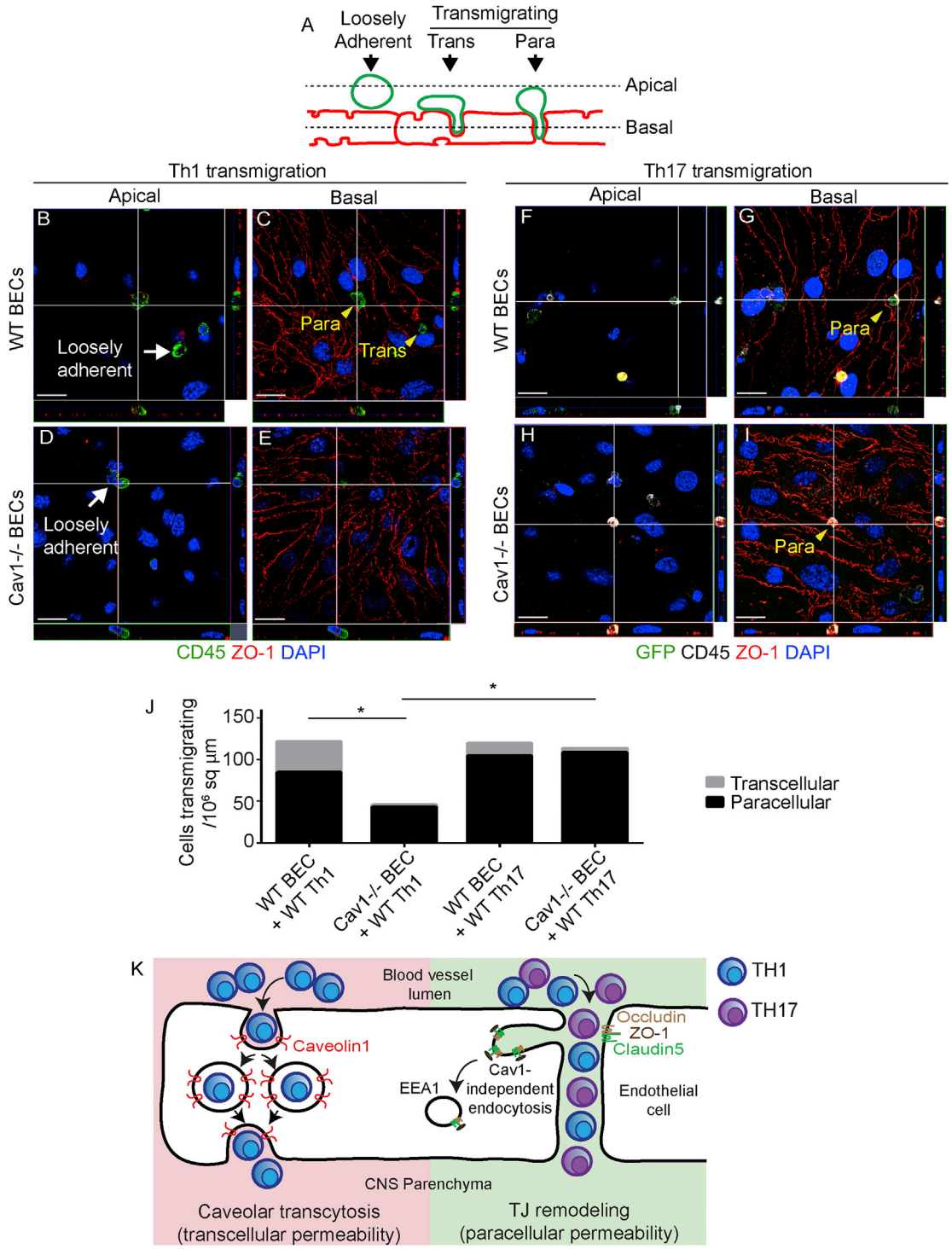

Figure 6. Endothelial Caveolin1 Promotes Th1, but Not Th17, Lymphocyte Transcellular Transmigration

(A) Schematic diagram of T cell transmigration states in the *in vitro* assay. Wild-type Th1 or *Rorc(γt)*$^{GFP/+}$ GFP^{+} Th17 cells were applied to monolayers of wild-type or *Cav1*$^{-/-}$ primary brain endothelial cells. Based on their positions relative to endothelial ZO-1 in confocal image stacks, T cells were scored as either loosely adherent (non-transmigrating) or transmigrating via transcellular or paracellular routes.

(B–E) Apical and basal confocal images and orthogonal views of Th1 *in vitro* transmigration assay immunostained for ZO-1 (red), CD45 (green), and DAPI (blue). Loosely adherent Th1 cells are indicated with white arrows and transmigrating Th1 cells are indicated with yellow arrowheads on wild-type brain endothelial cells (apical slice, B; basal slice, C) or *Cav1*$^{-/-}$ brain endothelial cells (apical slice, D; basal slice, E).

(legend continued on next page)

et al., 2005). Thus, regulatory mechanisms underlying endothelial barrier integrity and dysfunction in CNS diseases differ from those proposed for epithelial barriers of the intestine and endothelial cells in the lung (Günzel and Yu, 2013). The prevalence of dynamic protrusions at preclinical EAE (Figures 1G, 1H, and 1N) is consistent with the proposed role for neutrophils in promoting early BBB breakdown by secretion of proteolytic enzymes (Aubé et al., 2014; Carlson et al., 2008). The lateral border recycling compartment can serve as the organelle in which rapid remodeling of tight junction proteins occurs in brain endothelial cells *in vitro* as they encounter transmigrating monocytes (Winger et al., 2014). These organelles contain both adherens- and tight junction-associated proteins and may correspond to the tight junction protrusions observed by two-photon imaging in gut epithelial cells (Marchiando et al., 2010), brain endothelial cells in the ischemic brain (Knowland et al., 2014) and spinal cord during inflammation (Figure 1). We find that CFA and *pertussis* primes the BSCB for remodeling by enhancing the number of tight junction protrusions but is insufficient to induce tight junction dynamic remodeling (Figure 1) or caveolar transcytosis (Figure 4).

Our results also reveal a striking difference between the cell biological mechanisms of BBB disruption in mouse models of multiple sclerosis and ischemic stroke. In t-MCAO, caveolar density and albumin uptake in cortical endothelium are enhanced as early as 6 hr after reperfusion of an occluded vessel (Haley and Lawrence, 2017; Knowland et al., 2014). However, high fractions of endothelial tight junction protrusions and gaps associated with increased biocytin permeability are observed only 24–48 hr after reperfusion (Haley and Lawrence, 2017; Knowland et al., 2014). Therefore, the mechanisms that safeguard the transcellular endothelial barrier fail before those that regulate the paracellular barrier in ischemic stroke (Haley and Lawrence, 2017; Knowland et al., 2014). In contrast, paracellular permeability is an early and persistent feature of EAE, whereas transcellular permeability is only elevated during severe stages of the disease (Figures 3 and 4; Figure S4C). This mechanistic dichotomy for barrier breakdown during t-MCAO versus EAE may be due to either distinct inflammatory triggers or the timing when leukocyte subsets infiltrate the CNS in these two disorders (Lopes Pinheiro et al., 2016).

Our analysis reveals a role for caveolae in selective trafficking of specific T cell subtypes across the BSCB. We find that mice lacking caveolae (Razani et al., 2001) are partially protected from EAE, demyelination, and infiltration of INF-γ-producing Th1 subtypes into the spinal cord (Figure 5). Our data are consistent with a study showing that *Cav1*$^{-/-}$ mice are protected from EAE pathology and entry of T cells (Wu et al., 2016). However, in contrast to that study, we find that the numbers of CD4^{+} and Th17^{+} lymphocytes that infiltrate the CNS are unchanged between *Cav1*$^{-/-}$ and wild-type EAE mice (Wu et al., 2016). This discrepancy may be due to either interstrain genetic or microbiome differences between mice used in both studies. Our study employed *Cav1*$^{-/-}$ mice on a C57BL/6J background, whereas Wu et al. (2016) used C57BL/6N. Because ~0.8% of genes differ between these substrains (Zurita et al., 2011), genetic heterogeneity may contribute to the reported differences. It is known that commensal segmented filamentous bacteria (SFBs), present in BL/6N, drive Th17 differentiation (Ivanov et al., 2009) and confer susceptibility to autoimmune arthritis in BL/6J by enhancing IL-17A production (Wu et al., 2010), a cytokine that disrupts tight junctions (Kebir et al., 2007). The gut microbiome regulates maturation of the BBB (Braniste et al., 2014) and changes the phenotypic manifestation of cerebral cavernous malformations, a CNS vascular disease, in the same genetic background (Tang et al., 2017). These factors could contribute to differences in the phenotype observed between two studies in *Cav1*$^{-/-}$ EAE mice.

Previous studies have indicated unique temporal profiles of Th1 and Th17 effector cell infiltration into the CNS. Th17 cells are highest in the EAE spinal cord at 7 days post-immunization and decrease to baseline by day 10, whereas Th1 cells are low at day 10 and escalate in the EAE spinal cord at day 14 (Murphy et al., 2010). Consistently, adoptive transfer of Th17 cells that are differentiated *ex vivo* induces more rapid clinical presentation of disease compared with adoptive transfer of Th1 cells differentiated *ex vivo* (Rothhammer et al., 2011). Our finding that Cav1 is not required for early tight junction remodeling and early development of clinical EAE is consistent with caveolin-independent tight junction remodeling driving Th17 infiltration and disease initiation, followed by caveolar transcytosis driving Th1 infiltration and disease propagation. Our tracer experiments support this idea. The tight junction-permeant tracer biocytin-TMR crosses the BBB at early or mild EAE, whereas the transcellular tracer albumin crosses at severe stages of disease. Fibrinogen promotes *de novo* caveolae formation in brain endothelial cells (Muradashvili et al., 2014) and may contribute to enhanced transcellular permeability at severe EAE (Figure 4). Our findings suggest that efforts to inhibit caveolar transcytosis hold therapeutic potential to counter neuroinflammation in multiple sclerosis patients.

Why do Th1 cells preferentially cross the BSCB via caveolae during EAE? Cell adhesion molecules such as intercellular adhesion molecule 1 and 2 (ICAM-1/2) and vascular cell adhesion

(F–I) Apical and basal confocal images and orthogonal views of *Rorc(γt)*$^{GFP/+}$ Th17 (EGFP^{+}) *in vitro* transmigration assay immunostained for ZO-1 (red), GFP (green), CD45 (white), and DAPI (blue) on wild-type brain endothelial cells (apical slice, F; basal slice, G) or *Cav1*$^{-/-}$ brain endothelial cells (apical slice, H; basal slice, I). Scale bar, 10 μm.

(J) Stacked bar graph indicating numbers of transcellular and paracellular transmigrating Th1 or Th17 cells across wild-type or *Cav1*$^{-/-}$ brain endothelial cells. Significantly fewer Th1 cells transmigrate across *Cav1*$^{-/-}$ brain endothelial cells via either transcellular routes ($p < 0.05$) or paracellular routes ($p < 0.05$) compared with wild-type brain endothelial cells. Significantly fewer Th1 cells transmigrate across *Cav1*$^{-/-}$ brain endothelial cells compared with Th17 cells crossing *Cav1*$^{-/-}$ brain endothelial cells ($p < 0.05$).

(K) Model for lymphocyte trafficking across the BBB in EAE. Th1 cells preferentially deploy caveolae to cross the BSCB (transcellular permeability). In contrast, Th17 cells efficiently cross the BSCB through disrupted tight junctions (paracellular permeability), as well as caveolae. Tight junction remodeling involves formation of membrane invaginations (protrusions) that fuse with EEA1^{+} endosomes independently of caveolae.

See also Figure S5.

molecule 1 (VCAM-1) are enriched in caveolae and support transcellular migration by engaging infiltrating cell podocytes (Abadier et al., 2015; Carman and Martinelli, 2015; Millán et al., 2006). Th17 cells rely primarily on an αLβ2/ICAM-1 interaction (Rothhammer et al., 2011; Stromnes et al., 2008), whereas Th1 cells employ an α4/VCAM-1 complex for migration (Glatigny et al., 2011). Therefore, selective interactions between these adhesion molecules may direct Th1 cells more effectively toward caveolae when crossing the endothelium during neuroinflammation. We have recently shown that partial protection conferred by activation of Wnt/β-catenin signaling in the neurovasculature during EAE is associated with suppression of Caveolin1, VCAM-1, and T cell infiltration (Lengfeld et al., 2017). Our findings therefore suggest that inhibiting both tight junction degradation and caveolar transcytosis is a rationale for future therapies aimed at preventing immune cell entry into the CNS during autoimmune disease.

EXPERIMENTAL PROCEDURES

Mice

All experimental procedures were approved by Institutional Animal Care and Use Committee (IACUC) regulatory bodies at Columbia University Medical Center and the University of California, Irvine. Generation of transgenic *eGFP-Claudin5*$^{+/-}$ has been described (Knowland et al., 2014). *Cav1*$^{-/-}$ mice (Razani et al., 2001) and *Rorc(γt)*$^{GFP/+}$ mice (Ivanov et al., 2006) were obtained from the Jackson Laboratory (Maine). All mice were backcrossed to the C57BL/6J strain (Jackson Laboratory) for more than 8 generations.

EAE Induction

EAE was induced in 8- to 12-week-old female mice by subcutaneous immunization with a 100 μL emulsion of 100 μg of $MOG_{35–55}$ peptide (MEVG WYRSPFSRVVHLYRNGK) (Thermo Fisher Scientific) in PBS with CFA containing 200 μg of *Mycobacterium tuberculosis* H37Ra (Difco). The day of MOG immunization was designated as day 0. Mice received intravenous injections of 400 ng of *B. pertussis* toxin (List Biological Laboratories) 0 and 2 days post-immunization. Control animals received *B. pertussis* toxin and emulsion containing PBS/CFA without MOG. Mice were examined for clinical EAE signs using the following scale, with 0.5-point gradations for intermediate presentation: 0, no signs; 1, flaccid tail; 2, hindlimb paresis; 3, hindlimb paralysis; 4, hindlimb and forelimb paralysis; and 5, moribund (Lutz et al., 2012).

Laminectomy and *In Vivo* Two-Photon Imaging

Mice were anesthetized with 2.5% isoflurane in O_2 and maintained throughout surgery and imaging at 1.5% isoflurane in O_2 supplemented with subcutaneous carprofen (5 mg/kg) and lactated Ringer's solution. Body temperature was maintained at 37.5°C using a feedback-controlled homeothermic heating pad. Lumbar level 1 vertebra was removed, leaving the *dura mater* intact. A 3 mm borosilicate #0 coverslip was implanted on a bed of 1.5% agarose (in artificial cerebrospinal fluid) over the laminectomy site. The spinal column was stabilized using a custom-made titanium chamber affixed to adjacent vertebra with Vetbond and dental acrylic (Figure 1A). Intravital imaging was performed on a two-photon microscope (Sutter MOM) with a 920 nm excitation light (Mai Tai eHP Deep See, Spectra-Physics). Green fluorescence emission (Chroma 565 dcxr) was gathered using a 40× infrared objective (Olympus, 0.8 NA). ScanImage software (Pologruto et al., 2003) was used to acquire 60–150 μm optical stacks beneath the dura, sampled in 0.5 or 1 μm steps axially. Acquisition of each stack lasted 2–3 min. Repeated time-lapse acquisition was performed at intervals of ~45 min. Capillaries were identified by morphology (i.e., less than 2 endothelial cells across, <10 μm). Arterioles and venules were differentiated by direction of blood flow (arteriole > capillary > venule > median vein) and endothelial cell morphology (arterioles with elongated shape and venules with cobblestone shape) (Knowland et al., 2014). Image dimensions were 204.8 × 204.8 μm (512 × 512 pixels).

Tight Junction Remodeling Analysis

Images were analyzed with Fiji software (Schindelin et al., 2012) as described (Knowland et al., 2014). Optical slices in which the image was shifted by more than ~0.5 μm in the x or y plane or ~1 μm in the z plane because of motion artifacts were excised. Tight junction segments were defined as a continuous line between two endothelial cell borders without bifurcation. Tight junction segments were manually traced onto individual optical sections. Tight junction segments that were not visible at all time points were omitted from analysis. Protrusions were defined as EGFP-positive bulbous structures that extend >1 μm from the long axis of a tight junction segment (Figure 1C, yellow arrow). Protrusions not present at both the beginning and the end of the imaging session were considered dynamic (Figure 1, red arrows). Gaps were defined as tight junction segment discontinuities > 0.4 μm (Figure 1D). Tortuous strands were defined as tight junction segments with multiple curvilinear sections departing >1 μm from the long axis (Figure 1C). The number of protrusions, dynamic protrusions, gaps, and tortuous segments was measured for each optical z section.

BBB Permeability *In Vivo*

Thirty minutes after intravenous injection of 1% biocytin-TMR or albumin-Alexa Fluor 594 (Thermo Fisher Scientific), C57BL/6J, transgenic *eGFP-Claudin5*$^{+/-}$*; Cav1*$^{-/-}$ or *eGFP-Claudin5*$^{+/-}$ *Cav1*$^{-/-}$ mice were perfused with PBS and 4% paraformaldehyde (PFA). Tissues were post-fixed for 2–6 hr with 4% PFA, washed with PBS, cryoprotected in 30% sucrose overnight, embedded in optimal cutting temperature (OCT), and sectioned and immunostained for Glut1 (Calbiochem, 1:2,000) to visualize blood vessels, fibrinogen (LifeSpan Biosciences, 1:4,000) to visualize leakage across the BBB, and streptavidin-Alexa Fluor 594 (Thermo Fisher Scientific, 1:2,000) to visualize biocytin-TMR tissue distribution. Sections were imaged with a Zeiss LSM700 confocal microscope. Biocytin-TMR leakage was quantified as described (Knowland et al., 2014), by measuring the mean fluorescence intensity in spinal cord sections, and was presented as ratios to mean fluorescence intensities in liver sections. Three to six sections at thoracic spinal cord levels and three to six sections at lumbar spinal cord levels were quantified and averaged for each mouse. No significant differences in biocytin-TMR intensity within the liver were noted among groups. Fibrinogen-positive pixels were measured and divided by the area of the spinal cord section. Albumin-Alexa Fluor 594 uptake was measured as described (Knowland et al., 2014). Albumin-Alexa Fluor 594 single-channel images were uniformly thresholded, and pixels above the threshold were counted both within endothelial cells (endothelial-associated albumin) and outside of endothelial cells (parenchyma-associated albumin) (Figure 4).

T Cell Differentiation and Transmigration *In Vitro*

For Th1 cultures, splenocytes from C57BL/6 mice were collected 6 days after MOG immunization and cultured in Th1-polarizing conditions in the presence of antigen (20 μg/mL MOG plus 1 ng/mL IL-12, in RPMI supplemented with fetal bovine serum (FBS), L-glutamine, beta-mercaptoethanol, and non-essential amino acids) (Murphy et al., 2010). After 4 days, 5 ng/mL of IL-2 were added (Murphy et al., 2010). After 7 days in culture, production of the Th1 cytokine IFN-γ increased ~4,000% (Figure S5C) (data not shown). For Th17 cultures, splenocytes from *Rorc(γt)*$^{GFP/+}$ (Ivanov et al., 2006) were collected 6 days after MOG immunization and cultured in Th17-polarizing conditions with antigen: 20 μg/mL MOG, 10 ng/mL IL-1β, 30 ng/mL IL-6, 3 ng/mL transforming growth factor β (TGF-β), 10 μg/mL anti-IFN-γ, and 10 μg/mL anti-IL-4. After 4 days, 20 ng/mL of IL-23 were added. After 3 additional days, cells were restimulated with 0.5 μg/mL of plate-bound anti-CD3 and 0.5 μg/mL of soluble anti-CD28 (Cravens et al., 2016). Th17 cultures had ~4,000-fold increased production of IL-17 (Figure S5C). Th1 or Th17 cultures were applied to monolayers of primary mouse brain microvascular endothelial cells from wild-type or *Cav1*$^{-/-}$ mice (Cell Biologics) grown on collagen IV-coated glass-bottom plates in the presence of shear forces (10 dyn/cm^2 orbital rotation) and activated overnight with 1 ng/mL of tumor necrosis factor alpha (TNF-α) (Martinelli et al., 2014). In some experiments, brain endothelial cells were pretreated for 2 hr with caveola inhibitors genistein (Sigma, 400 μM), methyl-β-cyclodextrin (Sigma, 5 mM), or vehicle (Opti-MEM, Gibco). T cells were allowed to adhere and transmigrate for 90 min at 37°C, were washed 5× with warm Hank's balanced salt solution

(HBSS), were fixed with 4% PFA, and were immunostained with anti-CD4 or anti-CD45, anti-ZO-1, anti-GFP, and DAPI. An LSM700 confocal microscope equipped with a 40× water-immersion objective was used to determine positions of cells as superficial (adherent) or transmigratory (Martinelli et al., 2014). At least 50 cells per group were quantified across 6 wells per condition in three independent experiments.

Immunofluorescence and Antibodies

Rabbit anti-Caveolin1 (Calbiochem, 1:4,000), rat anti-CD4 (BD Pharmingen clone RM4-5, 1:100), rabbit anti-CD45 (Sigma, 1:250), rabbit anti-GFP (1:1,000), mouse anti-ZO-1 (Invitrogen, 1:1,000), mouse anti-CC1 (Santa Cruz, 1:200), rabbit anti-cleaved caspase-3 (Cell Signal, 1:250), rabbit anti-fibrinogen (LifeSpan Biosciences, 1:4,000), rabbit anti-Glut1 (Calbiochem, 1:2,000), and rabbit anti-laminin (Sigma, 1:4,000). Cells immunoreactive for CD4 inside the CNS parenchyma, and in meningeal and intraluminal spaces (delineated by laminin staining), were counted for six to eight thoracic spinal cord sections from each mouse. For unbiased measurement of myelinated areas, Fiji software was used to measure fluoromyelin-positive pixels (Thermo Fisher Scientific, 1:300) in uniformly thresholded images, which were expressed as a ratio of total white matter area.

Flow Cytometry

Spinal cords from wild-type and *Cav1*$^{-/-}$ mice 15 days post-immunization were homogenized between frosted glass slides. Mononuclear cells were isolated at the interphase of a 30%–70% Percoll gradient (GE Healthcare). Draining lymph nodes and spleens were mechanically homogenized, and red blood cells were lysed. Single-cell suspensions were restimulated for 5 hr *in vitro* with phorbol 12-myristate 13-acetate (PMA), ionomycin, brefeldin, and monensin (eBioscience). After F_c receptor blockade, cells were stained with Live-Dead Aqua (Invitrogen) plus antibodies against CD4-BV605 (BD Pharmingen), CD8-phycoerythrin (PE)Cy5 (BioLegend), CD45-BV421 (BD Pharmingen), and CD19-PECy7 (BD Pharmingen). Cells were then fixed, permeabilized, and stained for IL-17a-PE (BD Pharmingen) and IFN-γ-allophycocyanin (APC) (BD Pharmingen). Unstained CNS mononuclear cells were used for single-channel compensation, isotype controls, and fluorescence-minus-one controls.

Statistical Analysis

We performed two-way t tests for pairwise comparisons and one-way ANOVA followed by Newman-Keul's multiple comparison tests for group effects. EAE was assessed by two-way repeated-measure ANOVA followed by Sidak's multiple comparison test. EAE was analyzed in 34 wild-type and 32 *Cav1*$^{-/-}$ mice. Mice with no clinical disease presentation were included in the analysis (1 wild-type and 2 *Cav1*$^{-/-}$), and animals that died during the experiment were excluded from analysis (no wild-type and 2 *Cav1*$^{-/-}$). Statistical analyses were performed with GraphPad Prism software, and statistical significance for all figures is displayed as not significant (NS), $p > 0.05$, *$p < 0.05$, **$p < 0.01$, and ***$p < 0.001$.

SUPPLEMENTAL INFORMATION

Supplemental Information includes five figures and two movies and can be found with this article online at https://doi.org/10.1016/j.celrep.2017.10.094.

AUTHOR CONTRIBUTIONS

Conceptualization, S.E.L., S.P.G., and D.A.; Investigation, S.E.L., J.R.S., D.H.K., C.V.L.O., K.E., J.M.B., and D.A.; Resources, S.P.G. and D.A.; Writing – Original Draft, S.E.L., S.P.G., and D.A.; Writing – Review & Editing, S.E.L. and D.A.; Supervision, S.E.L., S.P.G., and D.A.; Funding, S.E.L., S.P.G., and D.A.

ACKNOWLEDGMENTS

We thank Tyler Cutforth, Celia F. Brosnan, and Cedric S. Raine for scientific and editorial input; Ilir Agalliu for statistical advice; and Adeela Syed from the UC Irvine Optical Biology Core for use of the LSM700 confocal microscope. S.E.L., J.R.S., and D.A. were supported by the NIH (R01 HL116995, R56 MH109987, and R01 MH112849), the National Multiple Sclerosis Society (NMSS) (RG4673A1/1 and FG2035-A-1), the Leducq Foundation (D.A.), and an unrestricted gift from John Castle to the Department of Neurology, Stroke Division, at CUMC (D.A.). D.H.K. and C.V.L.O. were supported by UC Irvine Undergraduate Research Opportunity (UROP) fellowships. S.P.G. was supported by a Searle Scholar Award, a Klingenstein fellowship, and an NMSS grant (RG4673A1/1). The Optical Biology Shared Resource of UC Irvine is funded by a Cancer Center support grant (CA-62203). The Columbia University Medical Center CCTI Flow Cytometry Core is supported in part by the Office of the Director, NIH (S10RR027050).

Received: May 26, 2017
Revised: September 16, 2017
Accepted: October 25, 2017
Published: November 21, 2017

REFERENCES

Abadier, M., Haghayegh Jahromi, N., Cardoso Alves, L., Boscacci, R., Vestweber, D., Barnum, S., Deutsch, U., Engelhardt, B., and Lyck, R. (2015). Cell surface levels of endothelial ICAM-1 influence the transcellular or paracellular T-cell diapedesis across the blood-brain barrier. Eur. J. Immunol. *45*, 1043–1058.

Al-Izki, S., Pryce, G., O'Neill, J.K., Butter, C., Giovannoni, G., Amor, S., and Baker, D. (2012). Practical guide to the induction of relapsing progressive experimental autoimmune encephalomyelitis in the Biozzi ABH mouse. Mult. Scler. Relat. Disord. *1*, 29–38.

Alvarez, J.I., Saint-Laurent, O., Godschalk, A., Terouz, S., Briels, C., Larouche, S., Bourbonnière, L., Larochelle, C., and Prat, A. (2015). Focal disturbances in the blood-brain barrier are associated with formation of neuroinflammatory lesions. Neurobiol. Dis. *74*, 14–24.

Aubé, B., Lévesque, S.A., Paré, A., Chamma, É., Kébir, H., Gorina, R., Lécuyer, M.A., Alvarez, J.I., De Koninck, Y., Engelhardt, B., et al. (2014). Neutrophils mediate blood-spinal cord barrier disruption in demyelinating neuroinflammatory diseases. J. Immunol *193*, 2438–2454.

Bartanusz, V., Jezova, D., Alajajian, B., and Digicaylioglu, M. (2011). The blood-spinal cord barrier: morphology and clinical implications. Ann. Neurol. *70*, 194–206.

Bennett, J., Basivireddy, J., Kollar, A., Biron, K.E., Reickmann, P., Jefferies, W.A., and McQuaid, S. (2010). Blood-brain barrier disruption and enhanced vascular permeability in the multiple sclerosis model EAE. J. Neuroimmunol. *229*, 180–191.

Braniste, V., Al-Asmakh, M., Kowal, C., Anuar, F., Abbaspour, A., Tóth, M., Korecka, A., Bakocevic, N., Ng, L.G., Kundu, P., et al. (2014). The gut microbiota influences blood-brain barrier permeability in mice. Sci. Transl. Med. *6*, 263ra158.

Brown, W.J. (1978). The capillaries in acute and subacute multiple sclerosis plaques: a morphometric analysis. Neurology *28*, 84–92.

Bruewer, M., Utech, M., Ivanov, A.I., Hopkins, A.M., Parkos, C.A., and Nusrat, A. (2005). Interferon-gamma induces internalization of epithelial tight junction proteins via a macropinocytosis-like process. FASEB J. *19*, 923–933.

Carlson, T., Kroenke, M., Rao, P., Lane, T.E., and Segal, B. (2008). The Th17-ELR+ CXC chemokine pathway is essential for the development of central nervous system autoimmune disease. J. Exp. Med. *205*, 811–823.

Carman, C.V., and Martinelli, R. (2015). T lymphocyte-endothelial interactions: emerging understanding of trafficking and antigen-specific immunity. Front. Immunol. *6*, 603.

Chang, S.H., Feng, D., Nagy, J.A., Sciuto, T.E., Dvorak, A.M., and Dvorak, H.F. (2009). Vascular permeability and pathological angiogenesis in caveolin-1-null mice. Am. J. Pathol. *175*, 1768–1776.

Cheng, J.P., and Nichols, B.J. (2016). Caveolae: one function or many? Trends Cell Biol. *26*, 177–189.

Claudio, L., and Brosnan, C.F. (1992). Effects of prazosin on the blood-brain barrier during experimental autoimmune encephalomyelitis. Brain Res. *594*, 233–243.

Cravens, P.D., Hussain, R.Z., Miller-Little, W.A., Ben, L.H., Segal, B.M., Herndon, E., and Stüve, O. (2016). IL-12/IL-23p40 is highly expressed in secondary lymphoid organs and the CNS during all stages of EAE, but its deletion does not affect disease perpetuation. PLoS ONE *11*, e0165248.

Cruz-Orengo, L., Daniels, B.P., Dorsey, D., Basak, S.A., Grajales-Reyes, J.G., McCandless, E.E., Piccio, L., Schmidt, R.E., Cross, A.H., Crosby, S.D., and Klein, R.S. (2014). Enhanced sphingosine-1-phosphate receptor 2 expression underlies female CNS autoimmunity susceptibility. J. Clin. Invest. *124*, 2571–2584.

Daneman, R., and Engelhardt, B. (2017). Brain barriers in health and disease. Neurobiol. Dis. *107*, 1–3.

Dileepan, T., Smith, E.D., Knowland, D., Hsu, M., Platt, M., Bittner-Eddy, P., Cohen, B., Southern, P., Latimer, E., Harley, E., et al. (2016). Group A *Streptococcus* intranasal infection promotes CNS infiltration by streptococcal-specific Th17 cells. J. Clin. Invest. *126*, 303–317.

Engelhardt, B., and Wolburg, H. (2004). Mini-review: transendothelial migration of leukocytes: through the front door or around the side of the house? Eur. J. Immunol. *34*, 2955–2963.

Fabis, M.J., Phares, T.W., Kean, R.B., Koprowski, H., and Hooper, D.C. (2008). Blood-brain barrier changes and cell invasion differ between therapeutic immune clearance of neurotrophic virus and CNS autoimmunity. Proc. Natl. Acad. Sci. USA *105*, 15511–15516.

Glatigny, S., Duhen, R., Oukka, M., and Bettelli, E. (2011). Cutting edge: loss of α4 integrin expression differentially affects the homing of Th1 and Th17 cells. J. Immunol *187*, 6176–6179.

Günzel, D., and Yu, A.S. (2013). Claudins and the modulation of tight junction permeability. Physiol. Rev. *93*, 525–569.

Haley, M.J., and Lawrence, C.B. (2017). The blood-brain barrier after stroke: structural studies and the role of transcytotic vesicles. J. Cereb. Blood Flow Metab. *37*, 456–470.

Ivanov, I.I., McKenzie, B.S., Zhou, L., Tadokoro, C.E., Lepelley, A., Lafaille, J.J., Cua, D.J., and Littman, D.R. (2006). The orphan nuclear receptor RORgammat directs the differentiation program of proinflammatory IL-17+ T helper cells. Cell *126*, 1121–1133.

Ivanov, I.I., Atarashi, K., Manel, N., Brodie, E.L., Shima, T., Karaoz, U., Wei, D., Goldfarb, K.C., Santee, C.A., Lynch, S.V., et al. (2009). Induction of intestinal Th17 cells by segmented filamentous bacteria. Cell *139*, 485–498.

Kebir, H., Kreymborg, K., Ifergan, I., Dodelet-Devillers, A., Cayrol, R., Bernard, M., Giuliani, F., Arbour, N., Becher, B., and Prat, A. (2007). Human Th17 lymphocytes promote blood-brain barrier disruption and central nervous system inflammation. Nat. Med. *13*, 1173–1175.

Kirk, J., Plumb, J., Mirakhur, M., and McQuaid, S. (2003). Tight junctional abnormality in multiple sclerosis white matter affects all calibres of vessel and is associated with blood-brain barrier leakage and active demyelination. J. Pathol. *201*, 319–327.

Knowland, D., Arac, A., Sekiguchi, K.J., Hsu, M., Lutz, S.E., Perrino, J., Steinberg, G.K., Barres, B.A., Nimmerjahn, A., and Agalliu, D. (2014). Stepwise recruitment of transcellular and paracellular pathways underlies blood-brain barrier breakdown in stroke. Neuron *82*, 603–617.

Komarova, Y.A., Kruse, K., Mehta, D., and Malik, A.B. (2017). Protein interactions at endothelial junctions and signaling mechanisms regulating endothelial permeability. Circ. Res. *120*, 179–206.

Kovtun, O., Tillu, V.A., Ariotti, N., Parton, R.G., and Collins, B.M. (2015). Cavin family proteins and the assembly of caveolae. J. Cell Sci. *128*, 1269–1278.

Lampugnani, M.G., Bravi, L., and Dejana, E. (2015). The role of microvascular endothelial WNT signaling the formation of the blood brain barrier. Springerplus *4* (*Suppl 1*), L47.

Lengfeld, J.E., Lutz, S.E., Smith, J.R., Diaconu, C., Scott, C., Kofman, S.B., Choi, C., Walsh, C.M., Raine, C.S., Agalliu, I., and Agalliu, D. (2017). Endothelial Wnt/β-catenin signaling reduces immune cell infiltration in multiple sclerosis. Proc. Natl. Acad. Sci. USA *114*, E1168–E1177.

Lopes Pinheiro, M.A., Kooij, G., Mizee, M.R., Kamermans, A., Enzmann, G., Lyck, R., Schwaninger, M., Engelhardt, B., and de Vries, H.E. (2016). Immune cell trafficking across the barriers of the central nervous system in multiple sclerosis and stroke. Biochim. Biophys. Acta *1862*, 461–471.

Louveau, A., Plog, B.A., Antila, S., Alitalo, K., Nedergaard, M., and Kipnis, J. (2017). Understanding the functions and relationships of the glymphatic system and meningeal lymphatics. J. Clin. Invest. *127*, 3210–3219.

Lutz, S.E., Raine, C.S., and Brosnan, C.F. (2012). Loss of astrocyte connexins 43 and 30 does not significantly alter susceptibility or severity of acute experimental autoimmune encephalomyelitis in mice. J. Neuroimmunol. *245*, 8–14.

Marchiando, A.M., Shen, L., Graham, W.V., Weber, C.R., Schwarz, B.T., Austin, J.R., 2nd, Raleigh, D.R., Guan, Y., Watson, A.J., Montrose, M.H., and Turner, J.R. (2010). Caveolin-1-dependent occludin endocytosis is required for TNF-induced tight junction regulation in vivo. J. Cell Biol. *189*, 111–126.

Martinelli, R., Zeiger, A.S., Whitfield, M., Sciuto, T.E., Dvorak, A., Van Vliet, K.J., Greenwood, J., and Carman, C.V. (2014). Probing the biomechanical contribution of the endothelium to lymphocyte migration: diapedesis by the path of least resistance. J. Cell Sci. *127*, 3720–3734.

Millán, J., Hewlett, L., Glyn, M., Toomre, D., Clark, P., and Ridley, A.J. (2006). Lymphocyte transcellular migration occurs through recruitment of endothelial ICAM-1 to caveola- and F-actin-rich domains. Nat. Cell Biol. *8*, 113–123.

Miyawaki-Shimizu, K., Predescu, D., Shimizu, J., Broman, M., Predescu, S., and Malik, A.B. (2006). siRNA-induced caveolin-1 knockdown in mice increases lung vascular permeability via the junctional pathway. Am. J. Physiol. Lung Cell. Mol. Physiol. *290*, L405–L413.

Muradashvili, N., Khundmiri, S.J., Tyagi, R., Gartung, A., Dean, W.L., Lee, M.J., and Lominadze, D. (2014). Sphingolipids affect fibrinogen-induced caveolar transcytosis and cerebrovascular permeability. Am. J. Physiol. Cell Physiol. *307*, C169–C179.

Murphy, A.C., Lalor, S.J., Lynch, M.A., and Mills, K.H. (2010). Infiltration of Th1 and Th17 cells and activation of microglia in the CNS during the course of experimental autoimmune encephalomyelitis. Brain Behav. Immun. *24*, 641–651.

Nag, S. (2003). Ultracytochemical studies of the compromised blood-brain barrier. Methods Mol. Med. *89*, 145–160.

Nitta, T., Hata, M., Gotoh, S., Seo, Y., Sasaki, H., Hashimoto, N., Furuse, M., and Tsukita, S. (2003). Size-selective loosening of the blood-brain barrier in claudin-5-deficient mice. J. Cell Biol. *161*, 653–660.

Paul, D., Cowan, A.E., Ge, S., and Pachter, J.S. (2013). Novel 3D analysis of claudin-5 reveals significant endothelial heterogeneity among CNS microvessels. Microvasc. Res. *86*, 1–10.

Pfeiffer, F., Schäfer, J., Lyck, R., Makrides, V., Brunner, S., Schaeren-Wiemers, N., Deutsch, U., and Engelhardt, B. (2011). Claudin-1 induced sealing of blood-brain barrier tight junctions ameliorates chronic experimental autoimmune encephalomyelitis. Acta Neuropathol. *122*, 601–614.

Platt, M.P., Agalliu, D., and Cutforth, T. (2017). Hello from the other side: how autoantibodies circumvent the blood-brain barrier in autoimmune encephalitis. Front. Immunol. *8*, 442.

Pologruto, T.A., Sabatini, B.L., and Svoboda, K. (2003). ScanImage: flexible software for operating laser scanning microscopes. Biomed. Eng. Online *2*, 13.

Raine, C.S., Cannella, B., Duijvestijn, A.M., and Cross, A.H. (1990). Homing to central nervous system vasculature by antigen-specific lymphocytes. II. Lymphocyte/endothelial cell adhesion during the initial stages of autoimmune demyelination. Lab. Invest. *63*, 476–489.

Razani, B., Engelman, J.A., Wang, X.B., Schubert, W., Zhang, X.L., Marks, C.B., Macaluso, F., Russell, R.G., Li, M., Pestell, R.G., et al. (2001). Caveolin-1 null mice are viable but show evidence of hyperproliferative and vascular abnormalities. J. Biol. Chem. *276*, 38121–38138.

Reese, T.S., and Karnovsky, M.J. (1967). Fine structural localization of a blood-brain barrier to exogenous peroxidase. J. Cell Biol. *34*, 207–217.

Reijerkerk, A., Kooij, G., van der Pol, S.M., Leyen, T., van Het Hof, B., Couraud, P.O., Vivien, D., Dijkstra, C.D., and de Vries, H.E. (2008). Tissue-type plasminogen activator is a regulator of monocyte diapedesis through the brain endothelial barrier. J. Immunol *181*, 3567–3574.

Rosengren, B.I., Rippe, A., Rippe, C., Venturoli, D., Swärd, K., and Rippe, B. (2006). Transvascular protein transport in mice lacking endothelial caveolae. Am. J. Physiol. Heart Circ. Physiol. *291*, H1371–H1377.

Rostami, A., and Ciric, B. (2013). Role of Th17 cells in the pathogenesis of CNS inflammatory demyelination. J. Neurol. Sci. *333*, 76–87.

Rothhammer, V., Heink, S., Petermann, F., Srivastava, R., Claussen, M.C., Hemmer, B., and Korn, T. (2011). Th17 lymphocytes traffic to the central nervous system independently of α4 integrin expression during EAE. J. Exp. Med. *208*, 2465–2476.

Ryu, J.K., Petersen, M.A., Murray, S.G., Baeten, K.M., Meyer-Franke, A., Chan, J.P., Vagena, E., Bedard, C., Machado, M.R., Rios Coronado, P.E., et al. (2015). Blood coagulation protein fibrinogen promotes autoimmunity and demyelination via chemokine release and antigen presentation. Nat. Commun. *6*, 8164.

Santizo, R.A., Xu, H.L., Galea, E., Muyskens, S., Baughman, V.L., and Pelligrino, D.A. (2002). Combined endothelial nitric oxide synthase upregulation and caveolin-1 downregulation decrease leukocyte adhesion in pial venules of ovariectomized female rats. Stroke *33*, 613–616.

Schindelin, J., Arganda-Carreras, I., Frise, E., Kaynig, V., Longair, M., Pietzsch, T., Preibisch, S., Rueden, C., Saalfeld, S., Schmid, B., et al. (2012). Fiji: an open-source platform for biological-image analysis. 9, 676–682.

Schubert, W., Frank, P.G., Woodman, S.E., Hyogo, H., Cohen, D.E., Chow, C.W., and Lisanti, M.P. (2002). Microvascular hyperpermeability in caveolin-1 (−/−) knock-out mice. Treatment with a specific nitric-oxide synthase inhibitor, L-NAME, restores normal microvascular permeability in Cav-1 null mice. J. Biol. Chem. *277*, 40091–40098.

Shin, T., Kim, H., Jin, J.K., Moon, C., Ahn, M., Tanuma, N., and Matsumoto, Y. (2005). Expression of caveolin-1, -2, and -3 in the spinal cords of Lewis rats with experimental autoimmune encephalomyelitis. J. Neuroimmunol. *165*, 11–20.

Simmons, S.B., Liggitt, D., and Goverman, J.M. (2014). Cytokine-regulated neutrophil recruitment is required for brain but not spinal cord inflammation during experimental autoimmune encephalomyelitis. J. Immunol *193*, 555–563.

Song, L., Ge, S., and Pachter, J.S. (2007). Caveolin-1 regulates expression of junction-associated proteins in brain microvascular endothelial cells. Blood *109*, 1515–1523.

Stamatovic, S.M., Keep, R.F., Wang, M.M., Jankovic, I., and Andjelkovic, A.V. (2009). Caveolae-mediated internalization of occludin and claudin-5 during CCL2-induced tight junction remodeling in brain endothelial cells. J. Biol. Chem. *284*, 19053–19066.

Stromnes, I.M., Cerretti, L.M., Liggitt, D., Harris, R.A., and Goverman, J.M. (2008). Differential regulation of central nervous system autoimmunity by T(H)1 and T(H)17 cells. Nat. Med. *14*, 337–342.

Sun, Y., Hu, G., Zhang, X., and Minshall, R.D. (2009). Phosphorylation of caveolin-1 regulates oxidant-induced pulmonary vascular permeability via paracellular and transcellular pathways. Circ. Res. *105*, 676–685, 15, 685.

Tang, A.T., Choi, J.P., Kotzin, J.J., Yang, Y., Hong, C.C., Hobson, N., Girard, R., Zeineddine, H.A., Lightle, R., Moore, T., et al. (2017). Endothelial TLR4 and the microbiome drive cerebral cavernous malformations. Nature *545*, 305–310.

Tiruppathi, C., Song, W., Bergenfeldt, M., Sass, P., and Malik, A.B. (1997). Gp60 activation mediates albumin transcytosis in endothelial cells by tyrosine kinase-dependent pathway. J. Biol. Chem. *272*, 25968–25975.

Tonra, J.R., Reiseter, B.S., Kolbeck, R., Nagashima, K., Robertson, R., Keyt, B., and Lindsay, R.M. (2001). Comparison of the timing of acute blood-brain barrier breakdown to rabbit immunoglobulin G in the cerebellum and spinal cord of mice with experimental autoimmune encephalomyelitis. J. Comp. Neurol. *430*, 131–144.

Umeda, K., Ikenouchi, J., Katahira-Tayama, S., Furuse, K., Sasaki, H., Nakayama, M., Matsui, T., Tsukita, S., Furuse, M., and Tsukita, S. (2006). ZO-1 and ZO-2 independently determine where claudins are polymerized in tight-junction strand formation. Cell *126*, 741–754.

Winger, R.C., Koblinski, J.E., Kanda, T., Ransohoff, R.M., and Muller, W.A. (2014). Rapid remodeling of tight junctions during paracellular diapedesis in a human model of the blood-brain barrier. J. Immunol *193*, 2427–2437.

Wu, H.J., Ivanov, I.I., Darce, J., Hattori, K., Shima, T., Umesaki, Y., Littman, D.R., Benoist, C., and Mathis, D. (2010). Gut-residing segmented filamentous bacteria drive autoimmune arthritis via T helper 17 cells. Immunity *32*, 815–827.

Wu, H., Deng, R., Chen, X., Wong, W.C., Chen, H., Gao, L., Nie, Y., Wu, W., and Shen, J. (2016). Caveolin-1 is critical for lymphocyte trafficking into central nervous system during experimental autoimmune encephalomyelitis. J. Neurosci. *36*, 5193–5199.

Zurita, E., Chagoyen, M., Cantero, M., Alonso, R., González-Neira, A., López-Jiménez, A., López-Moreno, J.A., Landel, C.P., Benítez, J., Pazos, F., and Montoliu, L. (2011). Genetic polymorphisms among C57BL/6 mouse inbred strains. Transgenic Res. *20*, 481–489.